



Effect of organic capping agents on the optical and photocatalytic activity of mesoporous TiO₂ nanoparticles by sol–gel method

M. V. Arularasu¹

© Springer Nature Switzerland AG 2019

Abstract

In this work, the effect of capping agent effects on the structural, morphological, optical properties and photocatalytic removal of Rhodamine B (RhB) dye has been investigated. TiO₂ nanoparticles were synthesized by a simple, fast and eco-friendly sol–gel method, in the presence of various capping agents, including ethylenediamine, polyvinyl alcohol (PVA), ethylene glycol, glucose and valine. The obtained TiO₂ nanoparticles have been characterized by X-ray diffraction (XRD), energy dispersive X-ray analysis, high resolution scanning electron microscopy and transmission electron microscopy, UV–visible absorption and photoluminescence (PL) spectroscopy. XRD pattern reveals the polycrystalline nature of TiO₂ with anatase structure. The results revealed that the optical absorption band of TiO₂ nanoparticles varied by capping agents. PL spectra exhibited visible emissions due to the formation of defects in the band gap region of TiO₂ nanoparticles. The photocatalytic degradation of RhB dye by synthesized TiO₂ nanoparticles using different capping agents was investigated under UV irradiation and the results demonstrated that TiO₂ nanoparticles have appreciable photocatalytic activity for decomposing RhB dye when PVA was used as a capping agent. The results explained that the preparation of TiO₂ nanoparticles showed a high efficiency in the removal of organic dyes.

Keywords TiO₂ · UV-light · Photoluminescence · Capping agents · RhB dye · PVA

1 Introduction

Transparent semiconducting metal oxide with high quality crystalline shape and size have much attention among the researchers due to their unique physical and chemical properties [1]. They were utilized in numerous important industrial applications such as temperature sensor, solar energy conversion, gas sensor, photocatalysis and electrochemistry etc., due to their structural stability and properties are very different to those of bulk counterparts [2–5]. Transition metal oxides are well known photocatalysts owing to their ability to generate hole–electron pairs [6]. Titanium dioxide (TiO₂) is one of the most extensively studied materials due to its thermal stability and harmless nature. It is multi-functional, cheap abundant and low cost materials. TiO₂ is a n-type semiconductor [7] that can be formed in three different polymorphs rutile, brookite

and anatase [8, 9]. This different polymorphs exhibits different bandgap energies with 3.0 eV (rutile), 3.2 eV (anatase) and ≈3.2 eV (brookite) [9].

Various methods have been employed to synthesize metal oxide nanoparticles, such as microwave method [10], hydrothermal method [11], solid-state [12], solution route method [13], sol–gel method [14]. Among these methods, the sol–gel method has low a temperature for crystallization resulting in large crystalline size and small surface area. Although, the final product would contain high carbon content when organic reagents are used during the process. The solvents used for sol–gel preparation method can be classified into aqueous or organic methods. In organic method solvents like, ethanol, methanol or ethylene glycol is widely used as solvents for metal oxide preparation [15–17]. However, these organic solvents are costly, inflammable and dangerous to the environment.

✉ M. V. Arularasu, arulrs597@gmail.com | ¹Korakkar Siddha Hospital and Research Centre, Tiruvallur, Tamil Nadu 602 001, India.



In aqueous method, DI (deionized) water can be used as a solvent to form more stable, uniform and eco-friendly solution that is easy to prepare metal oxide nanoparticles [18]. Hydrothermal and precipitation methods have been used to synthesize semiconductor metal oxides directly from solution, which resulted in the formation of a various range of particle size powder. This process is the most well-known method for the production of various metal oxides. Even if this process is able to synthesize crystals of substances which are unstable near the melting point, and the ability to synthesize large crystals of high quality.

Up to date, various surface modifications of metal oxides has been investigated by various capping agents, such as triethanolamine [19], trioctylphosphine oxide [20], triethanolamine [21], gelatin [22], L-cysteine [23]. Functionalizing of TMOS surface by chemical agents can alter particle size, morphology, thermodynamic stability, optical properties, photocatalytic activity as well as antibacterial activity.

Various types of the photocatalyst can inhibit the quick recombination of electron–hole pairs through different mechanism [24, 25]. Among all, organic capped metal oxide semiconductor photocatalyst, more efficiently involved in the suppression of electron–hole recombination via Schottky barriers to the Fermi energy of the selected metals usually being lower than that of the semiconductors. Cozzoli et al. [26] synthesized TiO_2 in the presence of organic capping agents and compared

the photocatalytic behavior by using Uniblue A as a pollutant. The results indicated that the photocatalytic effect was higher in the sample with both anatase and rutile structure. This is due to transfer of electrons from the anatase phase to the rutile phase which reduced the excitons recombination. In the present work, the photocatalytic performance of five samples of TiO_2 nanoparticles was investigated by the photocatalytic degradation of RhB under UV–visible lighting. The structure, morphology, optical and photocatalytic activity of synthesized TiO_2 nanoparticles were investigated in detail.

2 Materials and methods

2.1 Sample preparation

Titanium isopropoxide (TIP) ($\text{Ti}(\text{OCH})(\text{CH}_3)_2)_4$) were used as precursors in the sol–gel process represented in Fig. 1. A 20 mL of solution titanium isopropoxide was added dropwise into the 25 mL of solution containing 15 mL of ammonium hydroxide and 10 mL of deionized water under constant stirring at 70 °C to form oxide network. Intended capping agents, i.e. ethylenediamine (EDA), PVA, EG, glucose and valine required concentration was added and stirring continued for proper mixing of the capping agent in the mixed TIP and ammonium hydroxide. After an hour concentrated nitric acid mixed with deionized water

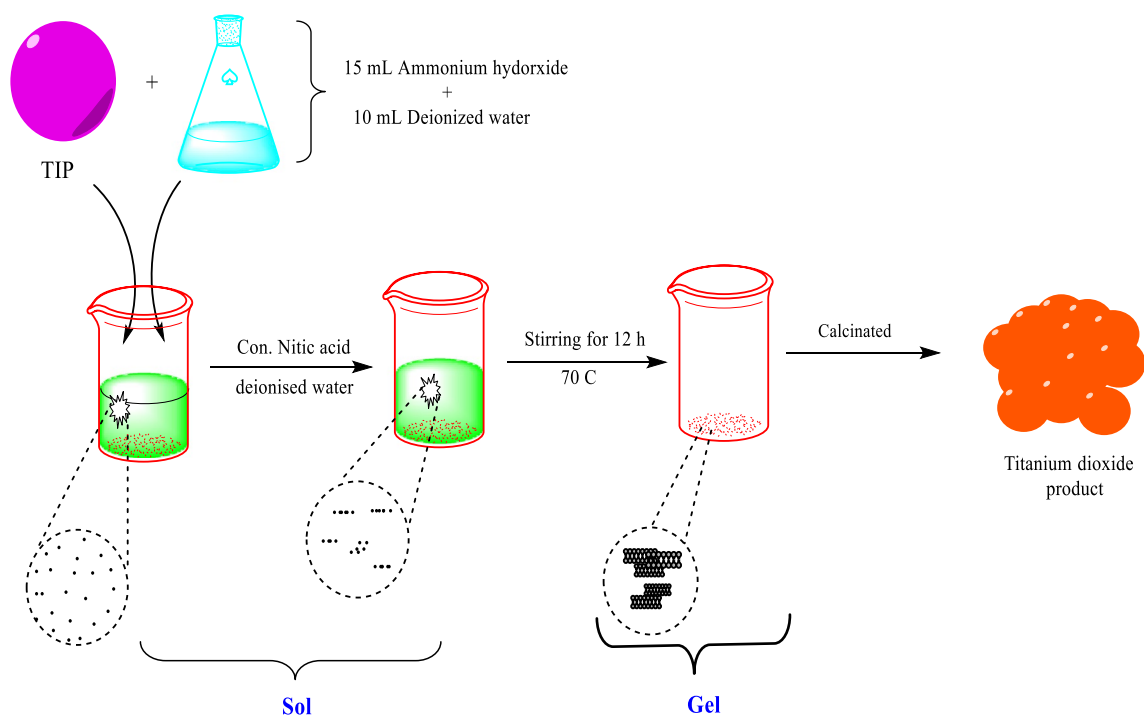
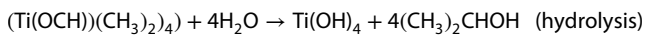
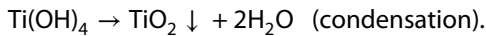


Fig. 1 Schematic diagram of preparation of TiO_2 nanoparticles by sol–gel method

was added into the titanium isopropoxide solution and keep it under constant stirring at 70 °C for 12 h highly viscous white sol–gel was obtained. The synthesized sol–gel was calcined for 2 h in a furnace at 500 °C for 1 h. Synthesis TiO₂ nanoparticles via sol–gel method is usually prepared by the reaction of hydrolysis and condensation of titanium alkoxide (TIP or Ti(OR)_n) to form titanium hydroxide.



In addition to alcohol, acid or base also helps hydrolysis of the precursor, which is transformed into titanium oxide network.



2.2 Characterization techniques

The X-ray diffraction (XRD) patterns of the sample were measured by using Philips X'pert PRO X-ray Diffractometer (PW3040/60) with CuK α radiation (45 kV, 40 mA). XRD patterns for the samples, examine were recorded in the region of 2θ ($= 10^\circ$ – 80°). The surface morphology and the size of the sample were characterized by (FESEM) Leica Cambridge S3600 and transmission electron microscopes (TEM) were taken with Philips CM12. The UV–visible optical absorption study was carried out using UV–visible spectrophotometer (Varian, Carry-50 Bio) in the wavelength range from 250 to 600 nm using quartz cuvette at room temperature. The excitation and photoluminescence (PL) spectra of the sample were measured by Perkin Elmer LS-45 luminescence spectrometer.

2.3 Photocatalytic experiment

To investigate the photocatalytic activity of the synthesized samples, degradation of RhB was performed under UV light irradiation at room temperature. A Hg lamp (UV) metal halide lamp with a 420 nm cutoff filter was used as the light source. An aqueous solution of RhB (100 mL 10 ppm) was prepared in a container and then 100 mg of the photocatalyst was dispersed in this solution. Before the irradiation, the catalyst/dye solution was kept in dark condition with constant magnetic stirring for 1 h to reach complete adsorption–desorption equilibrium. pH of the catalyst/dye solution was not adjusted. After 30 min intervals, 5 mL of the solution was taken and centrifuged to remove the photocatalyst particles before the photocatalytic experiment. The photo-reacted the solutions of the centrifuged sample were analyzed by measuring the change in absorption band maximum using the UV–visible spectrophotometer. After each photocatalytic reaction,

the same materials were being centrifuged and dried to recycle for another test.

3 Results and discussion

3.1 Structure and structural analysis

3.1.1 XRD

Powder XRD analysis was employed to characterize phase purity and the crystal structure of the synthesized photocatalyst TiO₂ samples shown in Fig. 2a–e [sample a (Glucose capped), sample b (Valine capped), sample c (EDA capped), sample d (EG capped), sample e (PVA capped) TiO₂ nanoparticles]. X-ray diffraction peaks of TiO₂ crystal appeared which could be easily indexed anatase TiO₂ (JCPDS file No. 86-1157) at 2θ angles of 24.14°, 35.36°, 35.56°, 35.73°, 47.52°, 54.79°, 55.21°, 61.36° are from (110), (103), (004), (112), (220), (105), (211), (204) planes. The intense and sharp peaks show that the sample is highly crystallinity and no other impurity peaks were detected in the XRD pattern of synthesized TiO₂ nanoparticles with capping agents, i.e. EDA, PVA, EG, glucose and valine, denote that the synthesized photocatalyst purity. The

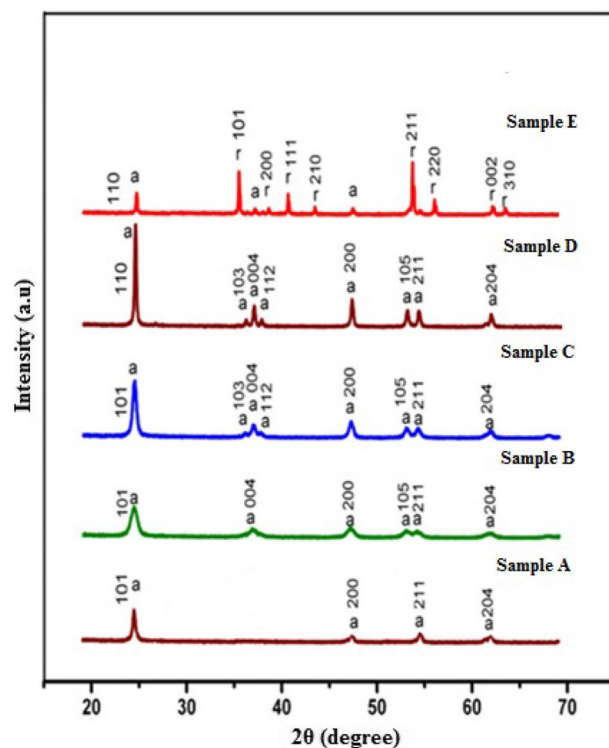


Fig. 2 XRD images of synthesized sample a (Glucose capped), sample b (Valine capped), sample c (EDA capped), sample d (EG capped), sample e (PVA capped) TiO₂ nanoparticles

crystallite size of TiO₂ nanoparticles was calculated by Scherrer's formula $0.9\lambda/\beta\cos\theta$ [27] shown in Table 1. Where λ is wavelength, of X-rays (1.540 for CuK α), β is the full width at half maximum, θ is the Bragg's angle.

3.1.2 FESEM

The representative morphology of synthesized mesoporous TiO₂ nanoparticles synthesized by sol–gel method was initially examined by FESEM. It is evident that the powder is more spherical like with various sizes. Although the particle sizes are reduced agglomerated, the grain boundaries between the crystallites are observable in synthesized samples. FESEM images of TiO₂ nanoparticles catalyst with added capping agents glucose and valine shown in Fig. 3a, b, which validate the nanoparticles presence of loosely agglomerate and disordered arrangement with the irregularity of gap among them. Reduced agglomerations of samples increase the available surface area on the sample and gradually increase the efficiency of the photocatalyst [28]. Figure 3c, d showed the very small fine particles of the samples with added capping agents EDA and EG. Figure 3e shows the mixture of nanoparticles with nanorods of TiO₂ nanoparticles was capped with PVA. However, TiO₂ nanoparticles with a surface modifier of PVA are higher particles form heavier particles and less agglomeration has occurred. The particle size appears to be stacked up to build due to the presence of oxygen vacancy at the synthesized sample with the higher surface to volume ratio [29, 30]. Elemental analysis of the synthesized sample was observed in the EDS spectrum. According to the Fig. 3f energy dispersive X-ray analysis (EDX) spectrum confirms the composition of the PVA capped TiO₂ and the absence of any impurities in the prepared sample.

3.1.3 TEM analysis

In the TEM images of the synthesized TiO₂ nanoparticle with a surface modifying agents include EDA, PVA, EG, glucose, and valine were conducted to discuss its particles nanorange and a spherical morphology shown in

Table 1 Crystal size and band gab of TiO₂ nanoparticles

Synthesized of TiO ₂ with different capping agents	Sample code	Crystal size (nm)	Band gap energy (eV)
Glucose	Sample A	64	3.25
Valine	Sample B	52	3.21
EDA	Sample C	33	3.20
EG	Sample D	19	3.17
PVA	Sample E	14	3.12

Fig. 4a–e. Figure 4a–d shows the presence of irregular spherical particles with sizes in the range of nanoparticles. Figure 4e which show the formation of nanorods, it depicted the irregular shape with good crystallinity with high accumulation which is contain nanoparticles with a diameter around 14 nm, which is consisted with XRD data and the selected area diffraction (SAED) pattern of TiO₂ sample has high crystallinity, nanosphere can be observed from Fig. 4f. The SAED pattern shown the crystalline structure of the synthesized sample and that the nanoparticles does not consist of single crystals, instead of aggregates of several single crystals.

3.1.4 Photoluminescence (PL) studies

The photoluminescence spectra are useful to disclose the efficiency of immigration, charge carrier trapping, and transfer and to understand the fate of electron–hole pairs in metal oxide nanoparticles since photoluminescence emission results from the recombination of free carriers [29, 30]. The correlation between morphology, size, and defect is investigated by photoluminescence spectra at room temperature. In Fig. 5 shown typical room temperature photoluminescence spectra of measporous TiO₂ nanoparticle with the excitation wavelength of 350 nm. The PL spectra peaks observed between 350 and 550 nm for all samples are due to inter-band gap defects like oxygen vacancies [31]. The PL intensity peaks around 389 nm associated with near band gap ultraviolet emission. The PL emission is observed at 438, 485 (blue emission), 510 and 527 (green emission) at room temperature. The strong peak at 485 nm corresponding to the blue emission, due to electron transitions intermediary by the vacancy levels in the band gap and oxygen defects [32, 33] formed during sample annealing at high temperature. The sample annealed at high-temperature structural defects, which generally act as the deep defect donors in semiconductor metal oxide that pitch into the optical emissions. The weak emission peak observed at 510 nm and 527 nm in green emission arises from a deeper level or trap course, emission is a particular ionized oxygen site with recombination of the photo-generated hole [34, 35]. The photoluminescence emission peak with a decreasing luminescence peak decrease in the particle size and increase in luminescence peak indicated is an increase in crystal size describe defects on the sample surface and consequently enhance the recombination process.

3.1.5 Band gap energy

The band gap energy of the sol–gel synthesized of TiO₂ are shown in Fig. 6. Absorption energy is around 316 nm, 390 nm, 420 nm, 460 nm and 478 nm for respective

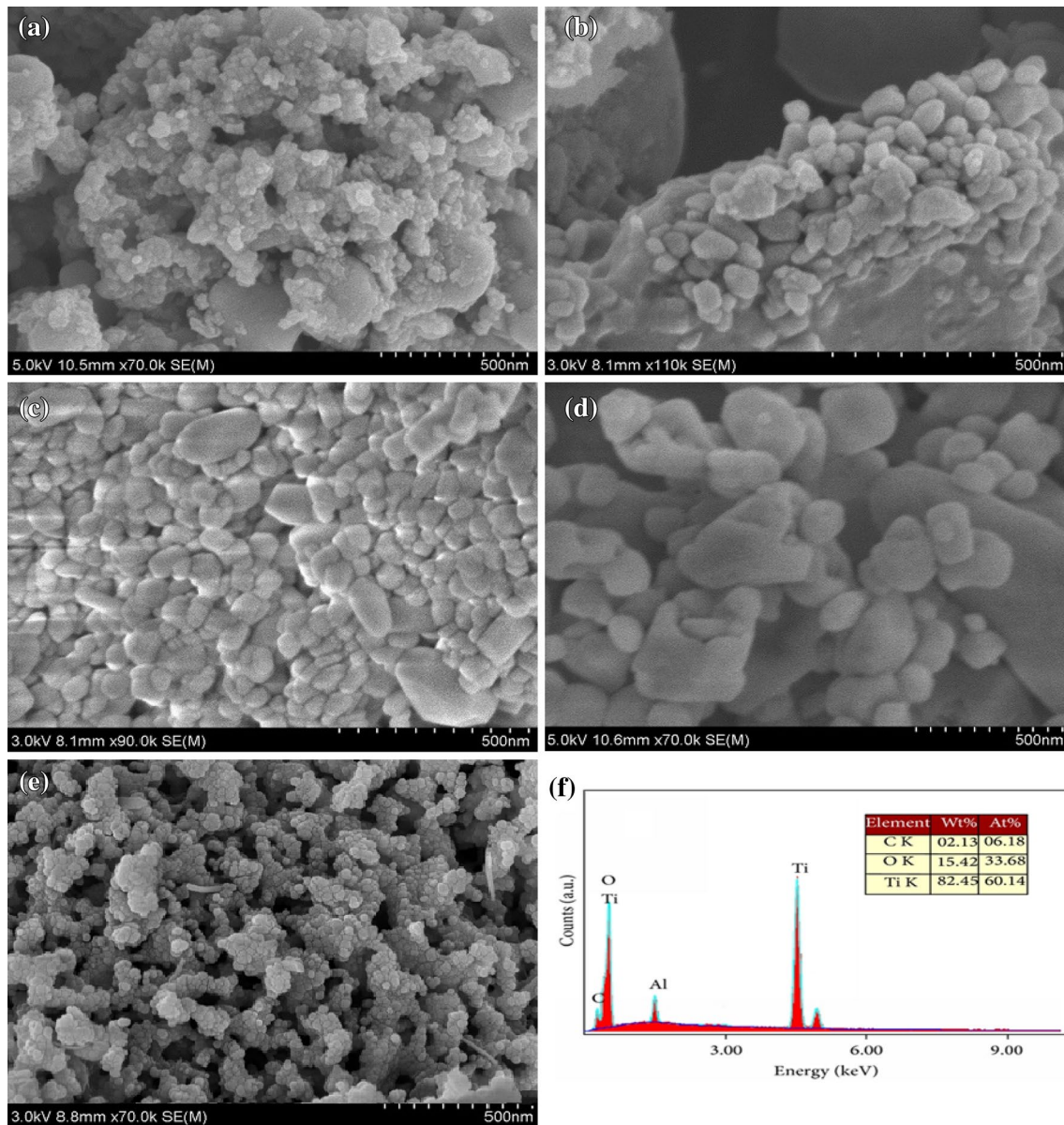


Fig. 3 FESEM images of sample **a** (Glucose capped), sample **b** (Valine capped), sample **c** (EDA capped), sample **d** (EG capped), sample **e** (PVA capped) TiO₂ nanoparticles, **f** EDX of PVA capped TiO₂ nanoparticles

glucose, valine, EDA, EG and PVA. An absorption edge position of EDA, EG and PVA capped TiO₂ photocatalyst shown towards longer wavelengths are compared to glucose and valine capped TiO₂ photocatalyst shifted towards lower wavelength. It can be undoubtedly attributed to the surface modifying agents, the absorption edge positions shift heading towards longer wavelength. The optical band gaps (E_g) of all the five samples were calculated by $(\alpha h\nu)^{1/2}$ versus $h\nu$, where α , h and ν are the absorption coefficient, Planck's constant and photo frequency respectively [36]. The band gap energy of

mesoporous TiO₂ nanoparticles shown in Table 1, which indicate that the TiO₂ nanoparticle capped with PVA band gap of 3.10 eV due to decreasing particle size on the increasing crystallinity of the sample. These results showed that the band gap energy of PVA capped TiO₂ nanoparticle by a sol-gel method using the TIP had shifted to a lower energy value. This decrease in the band gap may be associated with the increase in oxygen content due to the low heat treatment [37].

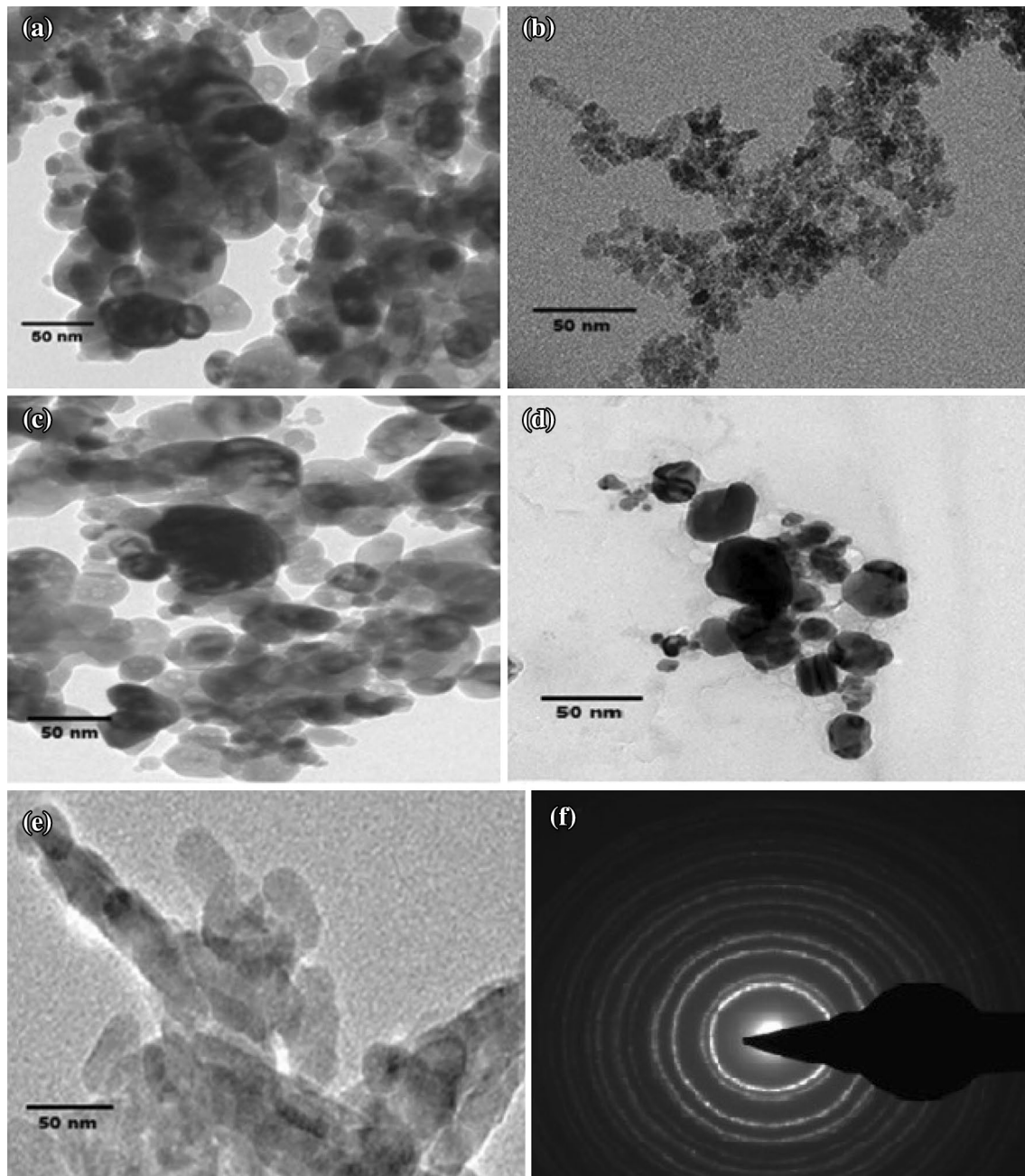


Fig. 4 TEM images of sample **a** (Glucose capped), sample **b** (Valine capped), sample **c** (EDA capped), sample **d** (EG capped), sample **e** (PVA capped) TiO_2 nanoparticles and **f** SAED pattern of TiO_2 nanoparticles

3.2 Photocatalytic studies

To study the photocatalytic activity of the synthesized TiO_2 photocatalyst, an experiment was carried out using an RhB solution as the probe material. Figure 7 shows the change in absorption spectra in the photo-catalytic degradation of RhB as a function of irradiation time. From the figure, the concentration of RhB gradually decreases as the exposure time increases for all samples. It can also

be seen the TiO_2 nanoparticle capped with PVA exhibit higher percentage degradation of RhB than other samples. Using photocatalytic calculations, mesoporous TiO_2 nanoparticle capped with PVA exhibit RhB degradation efficiency was 70% which were degraded subsequently at 120 min of irradiation time of ultraviolet light. The photocatalytic time scans of RhB illuminated at 502 nm with TiO_2 nanoparticle capped with PVA are depicted in Fig. 8. This indicates that the crystalline structure, nanosized

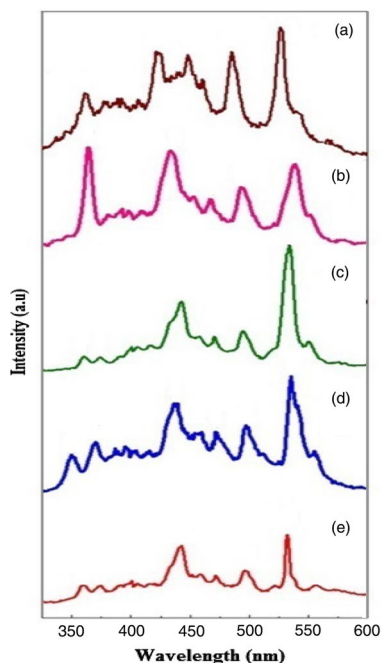


Fig. 5 PL emission spectra of sample a (Glucose capped), sample b (Valine capped), sample c (EDA capped), sample d (EG capped), sample e (PVA capped) TiO₂ nanoparticles

homogeneous granulometry and band gap is the important factor that affects the photocatalytic activity of the RhB. To study the stability of the TiO₂ nanoparticle sample to carry out five times recycle for RhB photodegradation test, as shown in Fig. 9. After five recycles, the catalyst did not show any significant loss of activity, thus indicating that the TiO₂ nanoparticle has outstanding stability.

The chemical and physical reactions for the degradation mechanism of RhB dye with TiO₂ nanoparticle under ultraviolet light irradiation shown below: Electron-hole pairs are generated on the synthesized metal oxide nanomaterial surfaces due to photoexcitation under visible light illumination [38, 39], as shown in Fig. 10. The mixed solution of RhB dye and photocatalyst is illuminated with ultraviolet light, the electrons in the lower valence band absorb energy and jump to the higher conduction band that had to the formation and development of positive hole and negative electron which move to the catalyst surface and act as active charge carriers [40]. Now this free electron (e⁻) will react with an adsorbed oxygen molecules (O₂) and forms oxygen radicals (O₂⁻). On the other hand, the holes (h⁺) of the valence band of TiO₂ nanoparticle are taken by OH⁻ derived from the aqueous solution and form hydroxyl radical (.OH) [41–43] in the mixed solution. As a result of this, radicals act as oxidizing agents. On the other hand, the reactive hydroxyl radical (.OH) can also be formed via the holes and OH⁻ ions in aqueous solution. These radicals (.OH, O₂⁻ and h⁺) can participate in the photooxidation reaction [44, 45]. Influence of sonication and light illumination conditions,

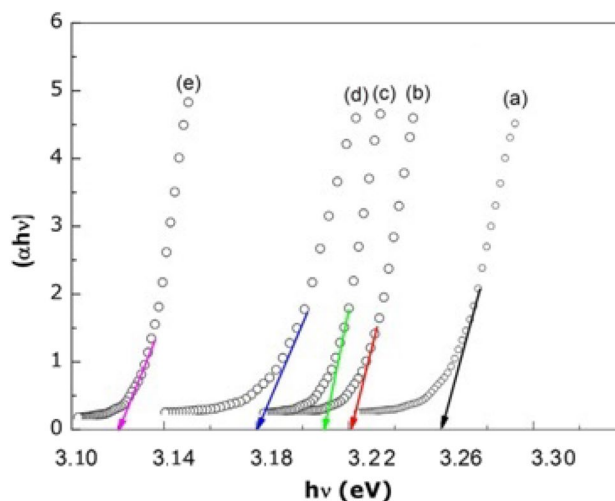


Fig. 6 UV-Vis absorption spectra of sample a (Glucose capped), sample b (Valine capped), sample c (EDA capped), sample d (EG capped), sample e (PVA capped) TiO₂ nanoparticles

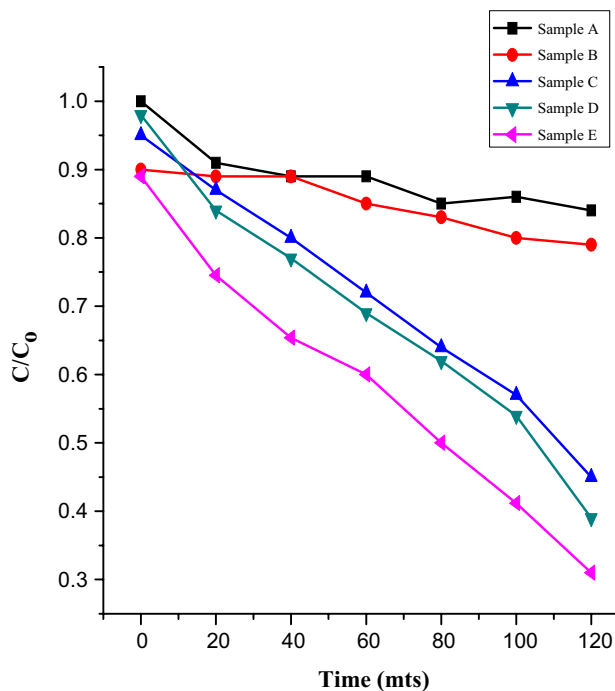


Fig. 7 Photocatalytic degradation of RhB under illumination of UV light using of synthesized sample a (Glucose capped), sample b (Valine capped), sample c (EDA capped), sample d (EG capped), sample e (PVA capped) TiO₂ nanoparticles

the RhB aqueous solution was decomposed into CO₂, H₂O and other small molecules due to the effective separation of photoexcited e⁻/hole [38, 44]. Various parameters such as particle size, phase composition, surface area and electron-hole recombination rate are to maximize the photocatalytic activity of synthesized samples. The recombination time of a free

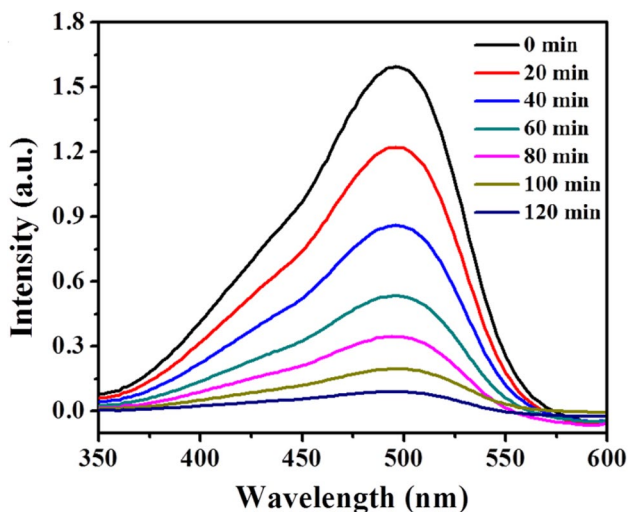


Fig. 8 The fluorescence intensity of TiO₂ nanoparticle at different time (sample E—PVA capped)

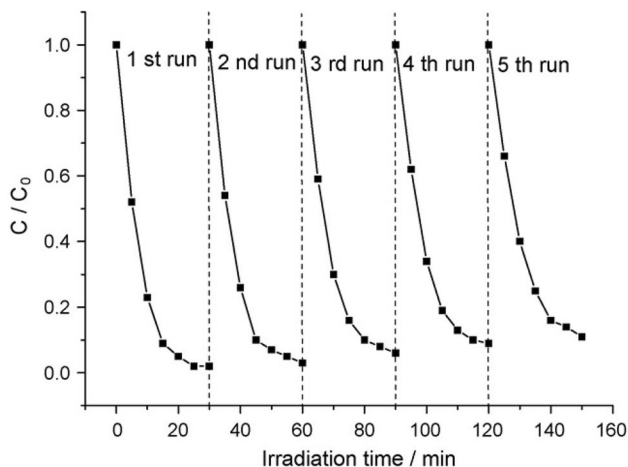


Fig. 9 The lifetime for photo-degradation of RhB by TiO₂ nanoparticle (sample E—PVA capped)

electron (e⁻) and the hole pairs (h⁺) is faster for commercial TiO₂ samples. The fast recombination of free electron (e⁻) and the hole pairs (h⁺) slow down the degradation process. In the higher photo-degradation of the TiO₂ nanoparticle capped with PVA (anatase phase) sample with a mixed dye solution, increase the density of free charge carriers by effective delay in the recombination time of photogenerated free electron (e⁻) and the hole pairs (h⁺) and decrease in band gap energy which improve the electron–hole recombination [46, 47]. Under the irradiation of TiO₂ nanoparticle, additional charge carriers further react with superoxide species and prevent the electron–hole recombination, and thus relatively increase degradation efficiency. The probable photocatalytic reaction mechanism of TiO₂ nanoparticle with an RhB dye molecule may be explained with the help of following equations.

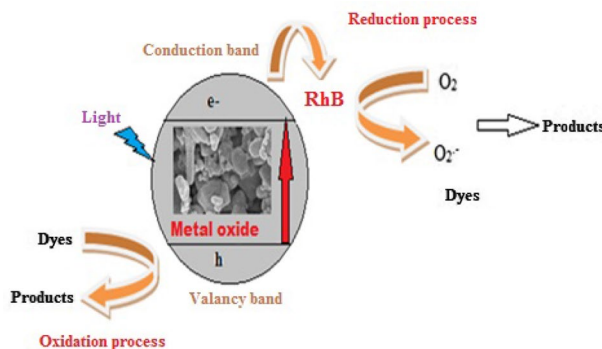
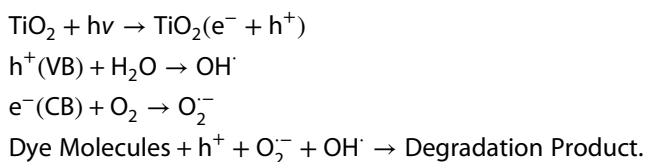


Fig. 10 Schematic diagram of general photocatalytic mechanism of TiO₂ nanoparticles



4 Conclusion

The potential UV light-driven photocatalytic activity of mesoporous TiO₂ nanoparticles synthesized by a sol–gel method for photodegradation of RhB dye. The UV–visible spectra showed that the band gap values of the photocatalyst decreased in the range 3.25–3.10 eV as capped with glucose, valine, EDA, EG and PVA. For rod-like TiO₂ nanoparticles, the enhanced intensity of the PL band in blue and green emission ranges results from the higher crystallinity, morphology, defects in surface gradually reduce the electron–hole recombination and consequently increase the photocatalytic degradation activity. The rod-like PVA capped mesoporous TiO₂ nanoparticles demonstrated rapid and efficient RhB dye decomposition with a degradation rate of 70% within the initial 120 min, owing to the higher adsorption capacity and the better electron–hole pair separation under UV light leads to the generation of less harmful chemicals.

Compliance with ethical standards

Conflict of interest The authors declare that they have no conflict of interest.

References

- Zhou Z, Lan C, Wei R, Ho JC (2019) Transparent metal-oxide nanowires and their applications in harsh electronics. *J Mater Chem C* 7:202–217

- Jiang Y, Bao C, Liu Q, Liang G, Lu M, Ma S (2018) A novel CeO₂-MoO₃-WO₃/TiO₂ catalyst for selective catalytic reduction of NO with NH₃. *Catal Commun* 103:96–100
- Liu G, Du K, Haussener S, Wang K (2016) Charge transport in two proton semiconducting structures solar fuels. *Chem Sus Chem* 9:2878–2904
- Lei Z, Xiong Z, Wang Y, Chen Y, Cao D, Zhao Y, Zhang J, Zheng C (2018) Photocatalytic reduction of CO₂ over facet engineered TiO₂ nanocrystals supported by carbon nanofibers under simulated sunlight irradiation. *Catal Commun* 108:27–32
- Liu L, Corma A (2018) Metal catalysts for heterogeneous catalysis: from single atoms to nanoclusters and nanoparticles. *Chem Rev* 118(10):4981–5079
- Ju Y, Wang M, Wang Y, Wang S, Fu C (2013) Electrical properties of amorphous titanium oxide thin films for bolometric application. *Adv Condens Matter Phys* 100:1–5
- Nadzirah S, Hashim U (2013) Effects of annealing temperature on current-voltage characteristics of TiO₂ thin film by sol-gel process on silicon substrate for biosensor application. In: 2013 IEEE regional symposium on micro and nanoelectronics (RSM), pp 167–170
- Pradhan SS, Pradhan SK, Bhavanasi V, Sahoo S, Sarangi SN, Anwar S, Barhai PK (2011) Low temperature stabilized rutile phase TiO₂ films grown by sputtering. *Thin Solid Films* 520:1809–1813
- Waghmode MS, Gunjal AB, Mulla JA, Patil NN, Nawani NN (2019) Studies on the titanium dioxide nanoparticles: biosynthesis, applications and remediation. *SN Appl Sci* 1:310–317
- Ragupathi C, Vijaya JJ, Narayanan S, John Kennedy L, Ramakrishnan S (2013) Catalytic properties of nanosized zinc aluminates prepared by green process using *Opuntia dilenii* haw palnt extract. *Chin J Catal* 34:1951–1958
- Hayashi H, Hakuta Y (2010) Hydrothermal synthesis of metal oxide nanoparticles in supercritical water. *Materials (Basel)* 3(7):3794–3817
- Patil SA, Shinde DV, Ahn DY, Patil DV, Tehare KK, Jadhav VV, Lee JK, Mane RS, Shrestha NK, Han S-H (2014) A simple, room temperature, solid-state synthesis route for metal oxide nanostructures. *J Mater Chem A* 2:13519–13526
- Chava RK, Kang M (2017) Improving the photovoltaic conversion efficiency of ZnO based dye sensitized solar cells by indium doping. *J Alloys Compd* 692:67–76
- Liu H, Liu G, Wang M, Li J, Liu Y, Cui H (2018) Building an interpenetrating network of Ni(OH)₂/reduced graphene oxide composite by a sol-gel method. *J Mater Sci* 53:15118–15129
- Sunde TOL, Garskaite E, Otter B, Fossheim HE, Saeterli R, Holmestad R, Einarsrud MA, Grande T (2012) Transparent and conducting ITO thin films by spin coating of an aqueous precursor solution. *J Mater Chem* 22:15740–15749
- Lee J, Lee S, Li G, Petruska MA, Paine DC, Sun S (2012) A facile solution-phase approach to transparent and conducting ITO nanocrystal assemblies. *J Am Chem Soc* 134:13410–13414
- Chen Z, Li W, Li R, Zhang Y, Xu G, Cheng H (2013) Fabrication of highly transparent and conductive indium-tin oxide thin films with a high figure of merit via solution processing. *Langmuir* 29:13836–13842
- Misra M, Hwang D-K, Kim YC, Myoung J-M, Lee TI (2018) Eco-friendly method of fabricating indium-tin-oxide thin films using pure aqueous sol-gel. *Ceram Int* 44:2927–2933
- Sathyamoorthy R, Mageshwari K, Mali SS, Priyadharshini S, Patil PS (2013) Effect of organic capping agent on the photocatalytic activity of MgO nanoflakes obtained by thermal decomposition route. *Ceram Int* 39:323–330
- Ma J (2011) Preparation and characterization of ZrO₂ nanoparticles capped by triethylphosphine oxide (TOPO). *J Wuhan Univ Tech Mater Sci Ed* 26(4):611–614
- Ayob MTA, Ahmad AR, Mohd HMK, Abdul Rahman I, Radiman S (2014) Effect of triethanolamine: ethylenediamine ratios on CuO nanoparticles prepared by ultrasound irradiation. In: AIP conference proceeding, vol 1614, pp 8–13
- Akhil K, Jayakumar J, Gayathri G, Khan SS (2016) Effect of various capping agents on photocatalytic, antibacterial and antibiofilm activities of ZnO nanoparticles. *J Photochem Photobiol B Biol* 160:32–42
- Rajabi HR, Farsi M (2016) Study of capping agent effect on the structural, optical and photocatalytic properties of zinc sulfide quantum dots. *Mater Sci Semicond Process* 48:14–22
- Jesudoss SK, Vijaya JJ, Selvam NCS, Kombariah K, Sivachidambaram M, Adinaveen T, John Kennedy L (2016) Effects of Ba doping on structural, morphological, optical, and photocatalytic properties of self-assembled ZnO nanospheres. *Clean Technol Environ Policy* 18:729–741
- Selvam NCS, Vijaya JJ, John Kennedy L (2013) Comparative studies on influence of morphology and La doping on structural, optical and photocatalytic properties of ZnO nanostructures. *J Colloids Interface Sci* 407:215–224
- Cozzoli PD, Comparelli R, Fanizza E, Curri ML, Agostiano A (2003) Photocatalytic activity of organic-capped anatase TiO₂ nanocrystals in homogeneous organic solutions. *Mater Sci Eng C* 23:707–713
- Arularasu MV, Sundaram R (2016) Synthesis and characterization of nanocrystalline ZnWO₄-ZnO composites and their humidity sensing performance. *Sens Bio-Sens Res* 11:20–25
- Sieland F, Schneider J, Bahnmann DW (2018) Photocatalytic activity and charge carrier dynamics of TiO₂ powders with a binary particle size distribution. *Phys Chem Chem Phys* 20:8119–8132
- Ansari SA, Khan MM, Kalathil S, Nisar A, Lee J, Cho MH (2013) Oxygen vacancy induced band gap narrowing of ZnO nanostructures by an electrochemically active biofilm. *Nanoscale* 5:9238–9246
- Ragupathi C, John Kennedy L, Vijaya JJ (2014) A new approach: synthesis, characterization and optical studies of nano-zinc aluminate. *Adv Powder Technol* 25:267–273
- Mbarek A (2018) Synthesis and visible-near-infrared photoluminescence emission of Er³⁺-doped LnP₅O₁₄ (Ln = La, Gd) ultraphosphates. *Inorg Chem Commun* 98:1–6
- Arularasu MV, Sundaram R, Magdalane CM, Kanimozhi K, Kaviyarasu K, Thema FT, Letsholathebe D, Maaza M (2017) Synthesis, humidity sensing, photocatalytic and antimicrobial properties of thin film nanoporous PbWO₄-WO₃ nanocomposites. *J Nanostruct* 7:47–56
- Arularasu MV, Anbarasu M, Poovaragan S, Sundaram R, Kanimozhi K, Magdalane CM, Kaviyarasu K, Thema FT, Mazza M (2018) Structural, optical, morphological and microbial studies on SnO₂ nanoparticles prepared by co-precipitation method. *J Nanosci Nanotechnol* 18:3511–3517
- Bhargava R, Sharma PK, Dutta RK, Kumar S, Pandey AC, Kumar N (2010) Synthesis and characterization of transition-metals-doped ZnO nanoparticles by sol-gel auto-combustion method. *Mater Chem Phys* 120:393–398
- Arularasu MV, Devakumar J, Sundaram R (2018) Impedance spectroscopy, magnetic and optical analysis of cadmium tungstate nanoparticles from influence of capping agent additives. *J Supercond Nov Magn* 9(31):2983–2990
- Kaviyarasu K, Ayeshamariam A, Manikandan E, Kennedy J, Lachumananandasivam R, Gomes UU, Jayachandran M, Maaza M (2016) Solution processing of CuSe quantum dots: Photocatalytic activity under RhB for UV and visible-light solar irradiation. *Mater Sci Eng B* 210:1–9
- Wang J, Wang Z, Huang B, Ma Y, Liu Y, Qin X, Zhang X, Dai Y (2012) Oxygen vacancy induced band-gap narrowing and

- enhanced visible light photocatalytic activity of ZnO. *ACS Appl Mater Interfaces* 4(8):4024–4030
38. Magdalane CM, Kaviyarasu K, Vijaya JJ, Siddhardha B, Jeyaraj B, Kennedy J, Maaza M (2017) Evaluation on the heterostructured $\text{CeO}_2/\text{Y}_2\text{O}_3$ binary metal oxide nanocomposites for UV/Vis light induced photocatalytic degradation of Rhodamine-B dye for textile engineering application. *J Alloys Compd* 727:1324–1337
 39. Magdalane CM, Kaviyarasu K, Vijaya JJ, Siddhardha B, Jeyaraj B (2016) Photocatalytic activity of binary metal oxide nanocomposites of CeO_2/CdO nanospheres: investigation of optical and antimicrobial activity. *J Photochem Photobiol B* 163:77–86
 40. Saranya J, Ranjith KS, Saravanan P, Mangalaraj D, Kumar RTR (2014) Cobaltdoped cerium oxide nanoparticles: enhanced photocatalytic activity under UV and visible light irradiation. *Mater Sci Semicond Process* 26:218–224
 41. Shanthi SI, Poovaragan S, Arularasu MV, Nithya S, Sundaram R, Magdalane CM, Kaviyarasu K, Maaza M (2018) Optical, magnetic and photocatalytic activity studies of Li, Mg and Sr doped and nndoped zinc oxide nanoparticles. *J Nanosci Nanotechnol* 18:5441–5447
 42. Xue C, Hu S, Chang Q, Li Y, Liu X, Yang J (2017) Fluoride doped $\text{SrTiO}_3/\text{TiO}_2$ nanotube arrays with a double layer walled structure for enhanced photocatalytic properties and bioactivity. *RSC Adv* 7:49759–49768
 43. Muniandy SS, Kaus NHM, Jiang Z-T, Altarawneh M, Lee HL (2017) Green synthesis of mesoporous anatase TiO_2 nanoparticles and their photocatalytic activities. *RSC Adv* 7:48083–48094
 44. Magdalane CM, Kaviyarasu K, Raja A, Arularasu MV, Mola GT, Isaev AB, Al-Dhabi NA, Arasu MV, Jeyaraj B, Kennedy J, Maaza M (2018) Photocatalytic decomposition effect of erbium doped cerium oxide nanostructures driven by visible light irradiation: investigation of cytotoxicity, antibacterial growth inhibition using catalyst. *J Photochem Photobiol B Biol* 185:275–282
 45. Kundu A, Mondal A (2019) Photodegradation of methylene blue under direct sunbeams by synthesized anatase titania nanoparticles. *SN Appl Sci* 1:280–297
 46. Arularasu MV, Devakumar J, Rajendran TV (2018) An innovative approach for green synthesis of iron oxide nanoparticles: characterization and its photocatalytic activity. *Polyhedron* 156:279–290
 47. Abdel-Messih MF, Ahmed MA, El-Sayed AS (2013) Photocatalytic decolorization of Rhodamine B dye using novel mesoporous $\text{SnO}_2\text{-TiO}_2$ nano mixed oxides prepared by sol-gel method. *J Photochem Photobiol A* 260:1–8

Publisher's Note Springer Nature remains neutral with regard to jurisdictional claims in published maps and institutional affiliations.